Inorganic Chemistry

Article

pubs.acs.org/IC

Structural and Magnetic Studies of a New Co(II) Thiocyanato Coordination Polymer Showing Slow Magnetic Relaxations and a Metamagnetic Transition

Susanne Wöhlert,[†] Tomasz Fic,[‡] Zbigniew Tomkowicz,[‡] Stefan G. Ebbinghaus,[§] Michał Rams,[‡] Wolfgang Haase,[∥] and Christian Näther*[,†]

[†]Institut für Anorganische Chemie, Christian-Albrechts-Universität zu Kiel, Max-Eyth-Straße 2, 24118 Kiel, Germany

[‡]Institute of Physics, Jagiellonian University, Reymonta 4, 30-059 Kraków, Poland

[§]Institut für Chemie, MLU Natur. Fakultät II, 06099 Halle/Saale, Germany

[∥]Eduard-Zintl-Institut für Anorganische und Physikalische Chemie, Technische Universität Darmstadt, Petersenstrasse 20, 64287 Darmstadt, Germany

Supporting Information

ABSTRACT: Reaction of $Co(NCS)_2$ with 4-ethylpyridine leads to the formation of three new compounds of composition $Co(NCS)_2$(4-ethylpyridine)$_4$ (**1**), $[(Co(NCS)_2]_2$(4-ethylpyridine)$_6$ (**2**), and $[Co(NCS)_2$(4-ethylpyridine)$_2]_n$ (**3**). In all compounds the coordination of the Co(II) ions is distorted octahedral. **1** consists of discrete monomeric complexes and in **2** two Co(II) cations are linked by pairs of μ-1,3-bridging thiocyanato ligands into dimers. In the crystal structure of **3** the Co(II) cations are connected into chains by the same bridge as in **2**. Magnetic studies show that **1** and **2** are paramagnets down to a temperature of 2 K, while compound **3**, which is the main object of this study, is an antiferromagnet with the Néel temperature T_N = 3.4 K. Its magnetic structure is built from ferromagnetic chains, which are weakly antiferromagnetically coupled. With increasing magnetic field a metamagnetic transition starts at ∼175 Oe, as observed for a polycrystalline sample. Magnetic relaxations, which were observed in the antiferromagnetic state, are retained at the metamagnetic transition. With decreasing field **3** remains in a state, in which except of the faster magnetic relaxation process in single chains also a slower process coexists resulting in the appearance of a magnetic hysteresis loop.

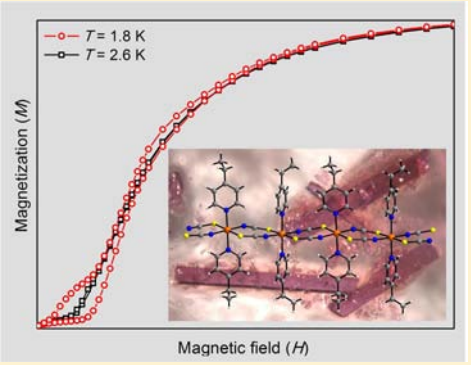

INTRODUCTION

Recently, investigations on a rational design of coordination polymers with desired magnetic properties has become of increasing interest. In this context compounds that show a slow relaxation of the magnetization and a hysteresis of molecular origin below a specific blocking temperature (T_B), like single molecule magnets (SMMs) or single chain magnets (SCMs), are of special importance because they are promising candidates for future applications such as, for example, ultrahigh density digital memories.[1] Whereas SMMs are known for more than two decades, the first SCM was experimentally realized in 2001 by Caneschi et al.[2] and therefore, this class of compounds is less investigated than SMMs. However, since that time an increasing number of contributions dealing with new SCM materials have been reported, and there are several excellent reviews in this field.[1a−d,3] For the preparation of such compounds cations with large magnetic anisotropy, like, for example, Co(II), Fe(II), or Mn(III), must be connected into chains by small-sized ligands that can mediate strong magnetic exchange interactions. The interchain interactions must be very small to prevent three-dimensional (3D) magnetic ordering.

Our scientific research focuses on the synthesis and magnetic properties of new transition metal coordination polymers with neutral N-donor coligands, in which the metal cations are linked by thio- or selenocyanate anions.[4] In this class of compounds different topologies of the metal thio- or selenocyanato coordination network are found but in most cases the metal cations are connected by two pairs of μ-1,3-bridging anionic ligands into chains, in which all ligands are trans-oriented.[5] These chains can be further connected into layers by bidentate coligands like, for example, pyrazine or pyrimidine which can mediate weak magnetic interactions. However, to simplify the situation we used the monodentate coligand pyridine in the synthesis, which leads to the formation of very simple compounds of composition $[M(NCS)_2(pyridine)_2]_n$ (M = Mn, Fe, Co, Ni, Cd), in which the metal cations are coordinated by two terminal *N*-bonded and trans-oriented pyridine ligands as well as two S- and two N-bonding μ-1,3-bridging thiocyanato anions (Figure 1).[6]

Received: May 21, 2013
Published: October 30, 2013

   dx.doi.org/10.1021/ic4012235 | *Inorg. Chem.* 2013, 52, 12947−12957

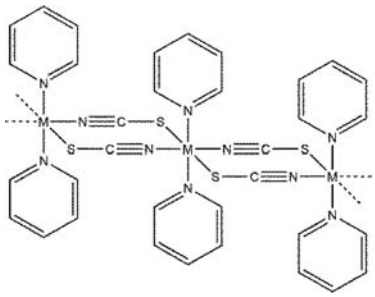

Figure 1. Sketch of the polymeric chains in compounds of composition $[M(NCS)_2(pyridine)_2]_n$.

Magnetic measurements of the Co compound reveal a slow relaxation of the magnetization, which was never observed before in a thiocyanato coordination polymer.[7] However, to investigate the influence of the anionic ligand on the magnetic properties we exchanged thio- by selenocyanate, and we found a significant increase in the effective energy barrier for spin reversal.[6a] Similar results were obtained on the layer compounds with 1,2-bis(4-pyridyl)ethylene as coligand,[8] that shows coexistence of antiferromagnetism and a slow relaxation of the magnetization as already reported by Miyasaka et al.[9] and Coulon et al.[10] We also investigated the influence of the metal cation and demonstrated that Fe(II) compounds can show a slow relaxation of the magnetization as well, even if such examples are rare.[11] The corresponding compound $[Fe(NCS)_2(pyridine)_2]_n$ was already reported by Foner et al. who found a metamagnetic transition (spin flip) in this compound at the critical field H_C = 1.1 kOe and T = 4.2 K.[12] We tried to increase the intrachain interactions by exchange of the thio- by selenocyanato anions which resulted in a compound that showed metamagnetism but above H_C a slow relaxation of the magnetization was observed.[11c]

Thus, compounds of this class form a rich family to study the influence of a chemical modification on the appearance of SCMs and generally on the magnetic behavior in detail. To study the influence of the coligand, we decided to prepare compounds based on cobalt(II) thiocyanate and 4-ethylpyridine. In the course of these investigations we obtained three compounds of different stoichiometry and structure. This includes a discrete complex of composition $Co(NCS)_2(4\text{-ethylpyridine})_4$ (**1**), a dimer of composition $[(Co(NCS)_2]_2(4\text{-ethylpyridine})_6$ (**2**), and the desired compound $[Co(NCS)_2(4\text{-ethylpyridine})_2]_n$ (**3**), which consists of chains. Magnetic measurements on **3** showed that both metamagnetism and slow relaxations occur, which is observed for the first time in a one-dimensional (1D) $Co(NCS)_2$ coordination polymer. Here we report on these investigations with the aim to shed a light on the nature of the magnetic relaxations in this compound.

SYNTHETIC AND STRUCTURAL INVESTIGATIONS

Synthetic Investigations. Different ratios of $Co(NCS)_2$ and 4-ethylpyridine were reacted in various solvents like water, methanol, ethanol, and acetonitrile. All of the obtained residues were investigated by elemental analysis, XRPD measurements, and IR-spectroscopy. Dependent on the stoichiometry and the solvent used different powder patterns are observed, indicating the formation of three different compounds. Elemental analysis reveals that for ratios of 1:4 and 1:2 between $Co(NCS)_2$ and 4-ethylpyridine a compound of composition $Co(NCS)_2(4\text{-ethylpyridine})_4$ (**1**) has formed and that a ratio of 1:1 leads to the formation of an 1:3 compound (1:3 = ratio between metal and coligand), which was later shown to be a dimer (**2**). If an excess of the metal salt is used in the synthesis (2:1 and 4:1) a ligand-deficient 1:2 compound of composition $Co(NCS)_2(4\text{-ethylpyridine})_2$ (**3**) is obtained. IR spectroscopic investigations show that in **1** only terminal *N*-bonded anions are present (ν_{as}(CN) = 2057 cm^{-1}), whereas two bands at 2064 cm^{-1} and 2108 cm^{-1} are found for the 1:3 compound **2** indicating that both, *N*-terminal and μ-1,3-bridging anions are present (Figure S1−S2 and Table S1 in the Supporting Information). For compound **3** an asymmetric stretching vibration at 2100 cm^{-1} is observed, which shows that only μ-1,3-bridging thiocyanato anions are present (Figure S3 and Table S1 in the Supporting Information). Unfortunately, X-ray Powder Diffraction (XRPD) investigations on **2** indicate that small amounts of compound **1** are always present, and this compound can also not be obtained phase pure by thermal decomposition. Later on we found that on very long reaction times even the dimer **2** can be obtained as a pure crystalline phase (Figure S4 in the Supporting Information). However, based on these results different crystallization experiments were performed in which single crystals of all three compounds were obtained (see Experimental Section). Crystalline powder of all compounds can be obtained by stirring the reactants in solution at room temperature, and a comparison of the experimental powder patterns with those calculated from single crystal data proves that these compounds are obtained as pure products (Figure S5−S7 in the Supporting Information).

Crystal Structures. $Co(NCS)_2(4\text{-ethylpyridine})_4$ (**1**) crystallizes in the triclinic space group $P\bar{1}$ with four formula units in the unit cell (Table 2). The asymmetric unit consists of two crystallographic independent cobalt(II) cations, four thiocyanato anions, and eight 4-ethylpyridine ligands, all of them located on general positions. In the crystal structure each cobalt(II) cation is coordinated by two terminal *N*-bonded thiocyanato anions and four *N*-bonded 4-ethylpyridine ligands in an octahedral geometry (Figure 2). The CoN_6 octahedra are slightly distorted with Co−N distances in the range of 2.071(4) Å to 2.206(3) Å for the first complex and 2.063(3) Å to 2.303(3) Å for the second cobalt complex. The angles around the first cobalt(II) cations are in the range of 88.1(2)° to 92.3(2)° and 177.23(13)° to 179.5(2)° while for the second Co they are in the range of 88.2(2) to 92.04(13) and 176.9(2) to

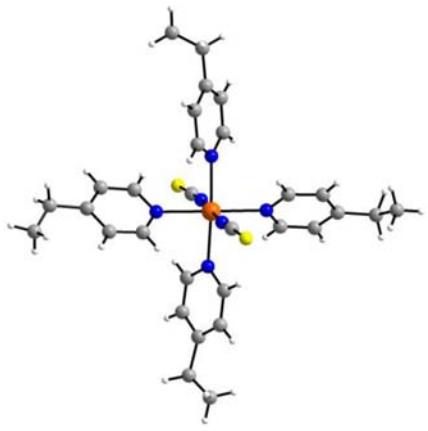

Figure 2. Molecular structure of one of the two crystallographically independent molecules of **1**. ORTEP plots of both molecules can be found in Figure S8 in the Supporting Information.

dx.doi.org/10.1021/ic4012235 | *Inorg. Chem.* 2013, 52, 12947−12957

178.9(2)° in the second complex (Table S2 in the Supporting Information).

$[(Co(NCS)_2]_2(4\text{-ethylpyridine})_6$ (**2**) crystallizes in the orthorhombic space group *Pbca* with four formula units in the unit cell (Table 2). The asymmetric unit consists of one cobalt(II) cation, two thiocyanato anions, and three 4-ethylpyridine ligands located on general positions. In the crystal structure each Co^{2+} cation is coordinated by one terminal *N*-bonded and two bridging thiocyanato anions and three *N*-bonded 4-ethylpyridine ligands within slightly distorted octahedra. The cobalt(II) cations are linked into dimers by pairs of μ-1,3-bridging thiocyanato anions, which are located on centers of inversion (Figure 3). The CoN_5S octahedra is

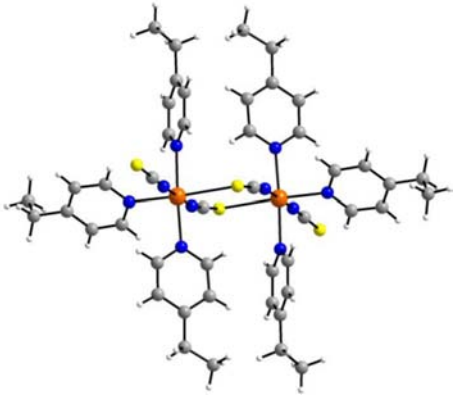

Figure 3. Molecular structure of the dimer in the crystal structure of **2**. An ORTEP plot of **2** can be found in Figure S9 in the Supporting Information.

slightly distorted with distances in the range of 2.053(3) Å to 2.6809(10) Å and angles between 85.6(1)° to 91.8(2)° as well as 176.7(1)° to 179.4(2)° (Table S3 in the Supporting Information).

$[Co(NCS)_2(4\text{-ethylpyridine})_2]_n$ (**3**) crystallizes in the monoclinic space group *Cc* with eight formula units in the unit cell (Table 2). The asymmetric unit consist of two cobalt(II) cations, four thiocyanato anions, and four 4-ethylpyridine ligands. In the crystal structure each cobalt(II) cation is coordinated by two N-atoms of the 4-ethylpyridine ligands, two *N*-bonded and two *S*-bonded thiocyanato anions in a slightly distorted octahedral geometry (Figure 4 and Table S4 in the Supporting Information).

The cobalt(II) cations are linked by thiocyanato anions into chains, which elongate in the direction of the crystallographic *a*-axis (Figure 4: top). The intrachain cobalt to cobalt separation through the thiocyanato anions are 5.62 Å and 5.65 Å. Within the chains the $N_{4\text{-ethylpyridine}}$-$N_{4\text{-ethylpyridine}}$ vectors of neighboring Co atoms are canted by 6.9°. The shortest interchain separation between the metal cations amounts to 8.31 Å. The chains are arranged into columns that elongate in the direction of the crystallographic *c*-axis, with the 4-ethylpyridine ligands in neighboring columns oriented nearly perpendicular, so that a "herringbone" structure is formed (Figure 4: bottom). The angle between the differently oriented $N_{ethylpyridine}$-$N_{ethylpyridine}$ of neighboring chains amounts 63.4° and 70.0°.

It is noted that we have found no example of a study in which the occurrence of a monomer, a dimer, and a chain for the same combination of transition metal thiocyanato and coligand was reported. However, the individual building blocks are well-known, and some examples are given in the reference list.[6c,13]

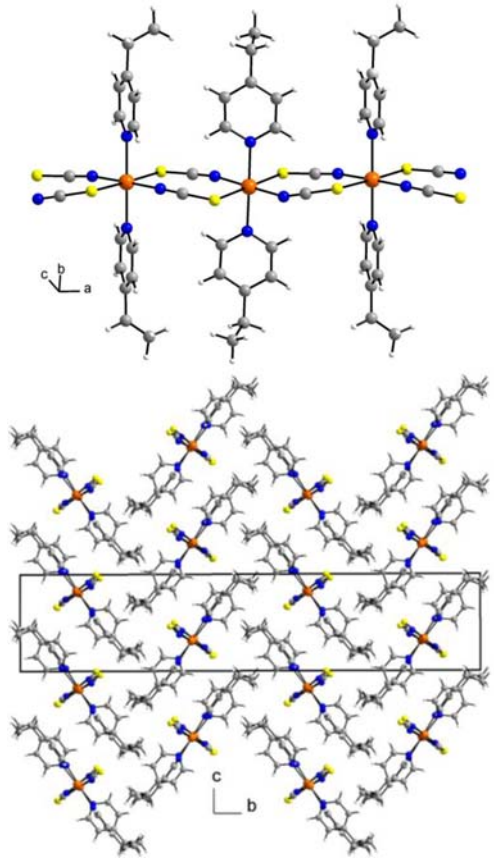

Figure 4. View of the Co(II) thiocyanato chains (top) and crystal structure of **3** viewed along the *a*-axis (bottom). An ORTEP plot of **3** can be found in Figure S10 in the Supporting Information.

MAGNETIC INVESTIGATIONS

DC Study. In this section the magnetic properties of compounds **1**, **2**, and **3** are presented that were measured on powder samples. The temperature dependence of the susceptibility $\chi(T)$ for compound **1** built from discrete complexes and of the dimer **2** is presented in Figure S11 in the Supporting Information. The effective magnetic moment $\mu_{eff} = (8\chi T)^{1/2}$ decreases with decreasing temperature, which is due to spin−orbit coupling as indicated by the room temperature value for μ_{eff} of 5.2 μ_B (**1**) and of 5.5 μ_B (**2**), thus larger than the spin only value 3.87 μ_B ($S = 3/2$), expected for a high-spin Co(II) ion.

In Figure 5 the temperature dependence of χ and of the χT product for **3** is shown as measured in field of 100 Oe. The susceptibility shows a sharp maximum at 3.2 K, which may be a manifestation of an antiferromagnetic phase transition due to an antiferromagnetic interchain coupling. The fast rise in the χT vs T curve below 20 K is consistent with ferromagnetic intrachain coupling. From these data the value of the effective magnetic moment (μ_{eff}) at high temperatures was determined to be 5.23 μ_B.

In Figure S12 in the Supporting Information the reciprocal temperature dependence of $\ln(\chi T)$ is shown. Its linear behavior above 5 K is compatible with an anisotropic (Ising like) 1D system. The deviation from linearity at lower temperatures is in accord with a small antiferromagnetic interchain coupling. The slope of this dependence (~11 K) is a measure of the magnetic correlation energy ($J/2$; see eq 2).

dx.doi.org/10.1021/ic4012235 | *Inorg. Chem.* 2013, 52, 12947−12957

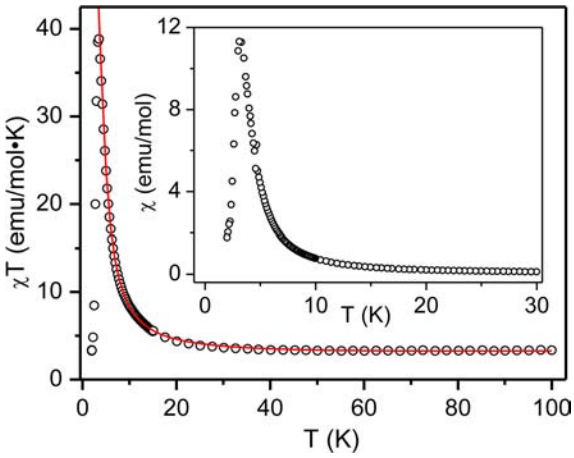

Figure 5. Temperature dependence of the χT product for **3** recorded in a DC magnetic field of 100 Oe. The red fitted line is extended outside the fitted region of 4−50 K. The inset shows the temperature dependence of χ.

As known, the low temperature magnetic behavior of the Co(II)-ion in an octahedral axially distorted coordination may be well described with the effective spin $s = 1/2$ and strongly anisotropic g factor. The Hamiltonian for the Ising chain of Co(II) ions in **3** is:

$$\mathcal{H} = -J\sum_{i,j} s_{i,z}s_{j,z} + \mu_B \sum_k \boldsymbol{H}\cdot\hat{g}\cdot\boldsymbol{s}_k \quad (1)$$

The solution of this Hamiltonian for the parallel and perpendicular susceptibility in a magnetic field close to zero was given by Fisher:[14]

$$\chi_{\parallel} = \frac{N_A\mu_B{}^2 g_{\parallel}{}^2}{4kT}\exp(J/2kT) \quad (2)$$

$$\chi_{\perp} = \frac{N_A\mu_B{}^2 g_{\perp}{}^2}{2J}\{\tanh(J/4kT) + J/[4kT\cosh^2(J/4kT)]\}\cdot \quad (3)$$

For powder samples the average susceptibility $\chi = 1/3(\chi_{\parallel} + 2\chi_{\perp})$ is measured. The experimental χT data were fitted with the Ising model in the temperature range 4−50 K (see Figure 5). In the fitting procedure also a constant ($\sim 500 \times 10^{-6}$ emu/mol) was added to the susceptibility to account for the temperature independent paramagnetism. The best fit parameters are: $J = +(25.2 \pm 0.4)$ K, $g_{\parallel} = 8.81 \pm 0.05$, $g_{\perp} \approx 0$, $zJ' = -(0.28 \pm 0.01)$ K. The parameter zJ' is a measure of the interchain interaction and was obtained including into the fitting procedure the following equation of the mean field theory[15]

$$\chi = \chi_{chain}\Big/\left(1 - \frac{zJ'}{2N_A g^2 \mu_B{}^2}\chi_{chain}\right) \quad (4)$$

where χ is the susceptibility of a system with weakly interacting chains and χ_{chain} is the susceptibility of isolated chains. In this context it is noted that the value of J obtained from the slope of the linear part of the $\ln(\chi T)$ vs reciprocal temperature curve (Figure S12 in the Supporting Information) is in good agreement with that obtained from the fit. The small difference originates from the antiferromagnetic interchain interaction.

$\chi(T)$ curves were registered in various magnetic DC fields H. It was observed that at H equal about 300 Oe, the maximum of $\chi(T)$ disappears and that at low temperatures a saturation of the magnetization $M(T) = \chi(T)H$ is reached (Figure 6). Therefore, it can be assumed that a metamagnetic transition occurs with a critical field which is somewhere below 300 Oe.

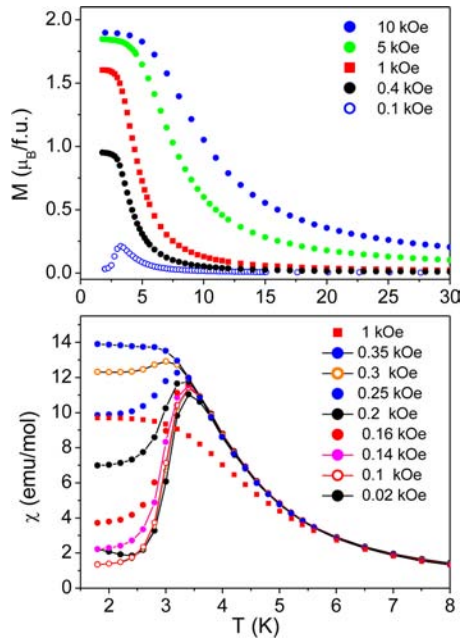

Figure 6. Magnetization (top) and susceptibility (bottom) vs temperature for **3** measured in various magnetic fields during cooling. The solid lines are only guides for the eye.

The field dependence of the magnetization $M(H)$ was measured at constant temperatures; see Figure 7. The inset to

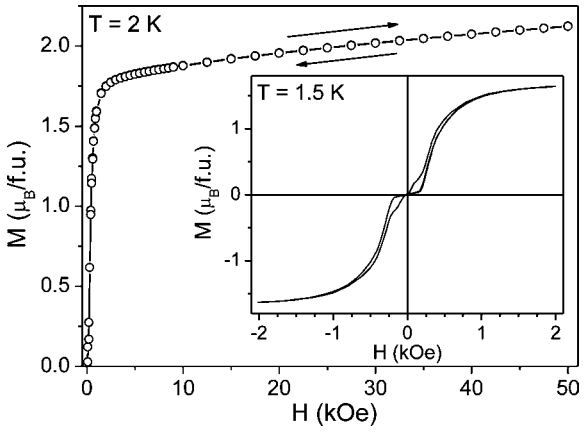

Figure 7. Main graph: magnetization loop of the powder sample of **3** measured at 2 K. Inset: magnetization loop measured at 1.5 K. The bottom branch of the loop overlaps with the virgin curve.

Figure 7 shows a $M(H)$ loop recorded at $T = 1.5$ K. A hysteresis is observed, but there is no remanence. It is also seen in the figure that with increasing field a jump of the magnetization occurs at some critical field H_C, which, determined from the maximum of the second derivative $\partial^2 M/\partial H^2$ after field (near the knee), is equal to 198 Oe. However, in fact the transition already starts earlier at about

dx.doi.org/10.1021/ic4012235 | Inorg. Chem. 2013, 52, 12947−12957

175 Oe. The fact that a metamagnetic transition occurs, can be understood on the basis of the crystallographic structure (see Figure 4), which consists of sets of ferromagnetic parallel chains with a weak antiferromagnetic coupling between them. It can be assumed that with increasing field the weakest antiferromagnetic interchain interaction is overcompensated, and the magnetic moments of neighbor chains reverse their orientation. This interchain interaction can be estimated by comparing the interchain exchange energy and the Zeeman energy

$$-zJ's^2 = g\mu_B sH_C \quad (5)$$

Substituting H_C = 175 Oe, s = 1/2, and $g = g_{\|}$ = 8.8 a value for zJ' of −0.4 K is obtained. Taking into account that this value is overestimated because instead of the internal field the external field was substituted into eq 5, the agreement with the value obtained from the Ising chain fit is relatively good. With zJ' = −0.3 K the ratio zJ'/J_{intra} amounts to $\sim -1 \times 10^{-2}$.

The magnetization curve was measured also in the greater field range up to ±50 kOe at 2 K and is shown in Figure 7 (main graph) in the field range of 0−50 kOe. No saturation is observed even in the highest field, which is consistent with a high anisotropy of Co(II) ions. In this scale the hysteresis is not seen. The details of the hysteresis loop near 0 kOe can be seen in Figure S13 in the Supporting Information.

It is seen that by decreasing the field the hysteresis loop does not close at H_C but remains open down to nearly zero field (Figure 7; inset). $M(H)$ curves recorded at different temperatures are shown in Figure S14 in the Supporting Information and the field derivative of the magnetization curves recorded at 2, 2.3, and 2.6 K are shown in Figure S15. Additional measurements were performed to see how the hysteresis loop depends on the maximum field applied to the sample (Figure S16 in the Supporting Information).

It was noted that the width of the hysteresis loop depended on the rate of the field change, which means that relaxations play a role. In further experiments the sample was magnetized to 1000 Oe, then the field was decreased to some determined value, and the magnetization was measured as a function of time t. Figure 8 presents exemplary dependences obtained for H = 80 and 300 Oe at 1.8 K.

To get more insight into the relaxation behavior, the $M(t)$ curves in Figure 8 were fitted with the stretched exponential

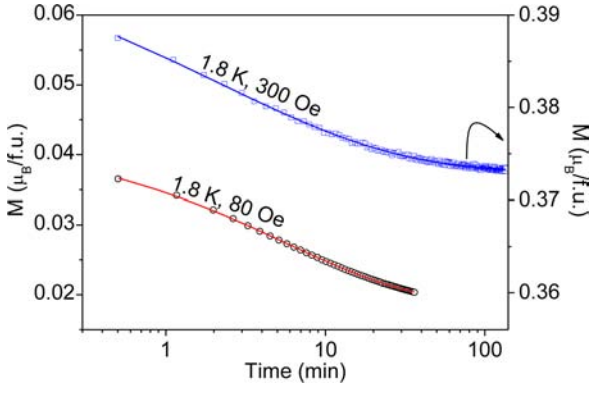

Figure 8. Time dependence of the magnetization after magnetizing the sample to 1000 Oe and decreasing the field to 80 or 300 Oe measured at a temperature of 1.8 K. Solid lines are fits to the stretched exponential. For this measurement the sample was frozen in Nujol.

$$M = M_0 + \Delta M e^{-(t/\tau)^{1-n}} \quad (6)$$

where τ is a median relaxation time, n is a measure of the distribution width of the relaxation times that can have values between 0 and 1, and M_0 is a final value to which M falls with time. For n a value of 0.5 ± 0.05 was obtained from fits. It is noted that for SCM compounds this value is typically not larger than 0.5.[3h] As checked for H = 80 Oe and T = 1.8, M values registered previously, that is, while increasing the field in the antiferromagnetic state, are not attainable. In other words, M_0 is greater than the corresponding M value from the bottom branch of the $M(H)$ loop. Thus, the metamagnetic transition in **3** is an irreversible process, at least in the time scale of experiment or longer.

It has been found that τ depends on the magnetic field and shows a maximum value (as checked for temperature 1.8 K) of 12 min at ∼150 Oe. This is the value at which the hysteresis loop is the widest. On the basis of this preliminary study it is not possible to state exactly whether this behavior is thermally activated. It is worth to note here that Coulon et al. studied an antiferromagnet with SCM relaxations and observed an enhancement of the relaxation time with field near the metamagnetic transition.[10]

The slow relaxations, described above, may also manifest themselves by FC vs ZFC bifurcations. To see these bifurcations the DC susceptibility was measured in various fields for the sample cooled in zero field (ZFC regime) and for the sample cooled in field (FC regime). Bifurcations of ZFC and FC curves were observed below and above H_C. In Figure 9

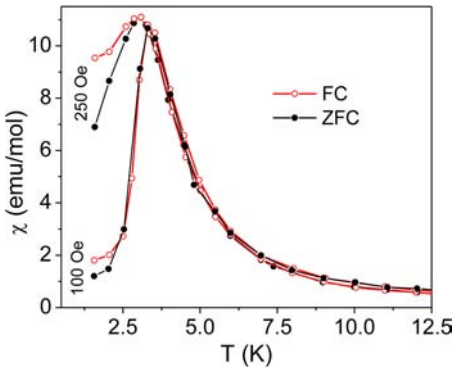

Figure 9. FC and ZFC $\chi_{DC}(T)$ curves measured in magnetic fields of 100 and 250 Oe.

only the data obtained for two fields are shown. With increasing field the bifurcations (FC vs ZFC splitting) grow at first, then decrease above 250 Oe but in 300 Oe they are still remarkable and disappear in higher field. The sample cooled in field 100 Oe should be still in the antiferromagnetic state (see Figure 6); however, as seen in Figure S16 in the Supporting Information, a small opening of the loop is observed already above 80 Oe. It follows that the bifurcations are related with the same process, which is responsible for the hysteresis loop in low field.

AC Study. AC susceptibility measurements were carried out to learn more about the relaxation properties of **3**. Figure 10 presents the temperature dependent AC data, registered at various constant frequencies in two DC bias field, one of which is close to zero, equal to 5 Oe, and the second one is above the critical field, equal to 600 Oe. For the data in other fields see Figure S17 in the Supporting Information.

dx.doi.org/10.1021/ic4012235 | Inorg. Chem. 2013, 52, 12947−12957

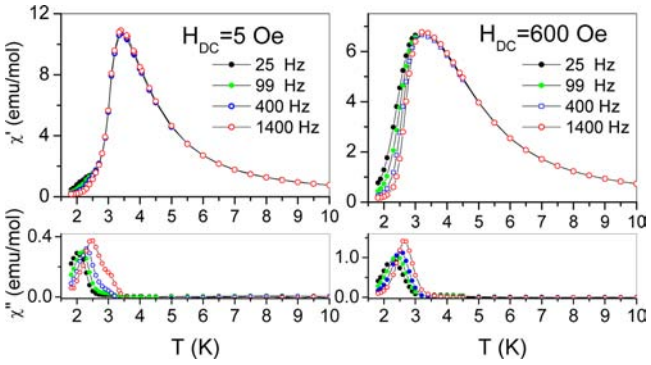

Figure 10. AC susceptibility vs temperature curves registered for **3** at various frequencies in two DC bias magnetic fields by H_{AC} amplitude of 3 Oe.

As seen, the maximum of χ' observed at 3.4 K in a field of 5 Oe does not shift with frequency and is not accompanied by a χ'' contribution at this temperature. This is in agreement with our interpretation that the analogous maximum in the DC susceptibility manifests the antiferromagnetic transition. However, a small frequency dispersion of both χ' and χ'' appears at lower temperatures near 2.5 K. It can be noticed by inspecting Figure S17 in the Supporting Information that the χ'' peak evolves with increasing DC field. It first increases, passes through a maximum, which is at about 200 Oe (cp. at the same frequencies), and decreases. This behavior corresponds to that shown in Figure 13 (see below), which presents DC field dependence of the AC susceptibility for the frequency of 10 Hz (these data will be used in the next section to build the phase diagram). With increasing field (above 600 Oe) it is observed that the peak of the $\chi'(T)$ curve moves to higher temperatures and the χ'' peak becomes very small, so a second χ'' peak emerges, which is clearly seen at 5 K for the measurement done in a field of 2 kOe and at 7.5 K for the measurement done in field of 5 kOe; see Figure S17 in the Supporting Information. The position of this χ'' peak is independent of the frequency. However, the χ' peak has no frequency dispersion at all. With increasing field both χ' and χ'' maxima shift to higher temperatures which is usually observed for ferromagnetic materials.

To determine relaxation times in **3**, the frequency dependent AC susceptibility $\chi_{AC}(f,T = \text{const})$ was measured at various temperatures and for two DC fields: of 5 Oe (below H_C) and 1000 Oe (above H_C). The data obtained are shown in Figure 11. The corresponding Argand's plots are presented in Figure S18 in the Supporting Information. Already at the first sight one can discern two relaxation processes taking place at 1000 Oe in some temperature range (clearly visible at 2.5 K in Figure S18 in the Supporting Information).

The data presented in Figure 11 were fitted with one ($\beta = 1$) or two Debye processes ($0 < \beta < 1$) using the generalized Debye formula:

$$\chi = \chi' - i\chi'' = \chi_\infty + (\chi_0 - \chi_\infty)\left\{\frac{\beta}{1 + (i\omega\tau_1)^{1-\alpha_1}} + \frac{1-\beta}{1 + (i\omega\tau_2)^{1-\alpha_2}}\right\} \quad (7)$$

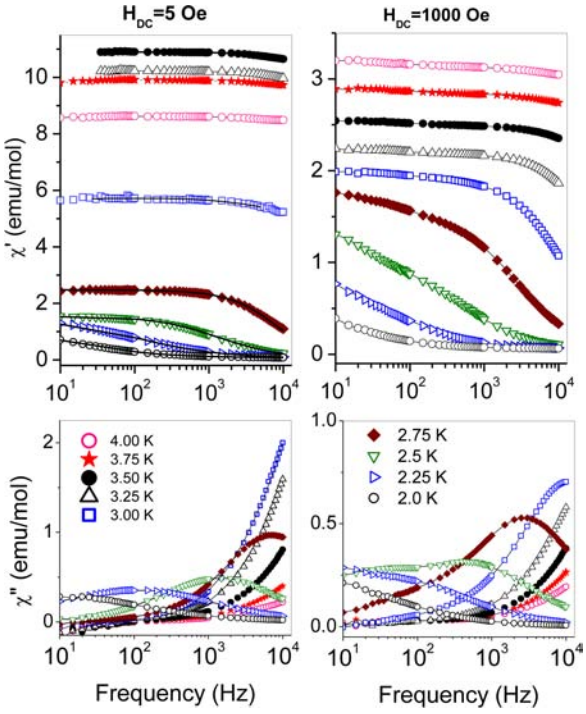

Figure 11. AC susceptibility vs frequency plots for **3** registered at various temperatures in 5 and 1000 Oe bias DC magnetic fields.

after separation of its complex form into χ' and χ'' components. The meaning of the symbols is the following: χ_0 and χ_∞ are susceptibilities in the limit of 0 Hz and in the limit of infinite frequency, respectively, τ_1, τ_2 are the relaxation times, and α_1, α_2 are parameters related with the widths of the relaxation times distributions ($0 \le \alpha \le 1$). Both AC susceptibility components (χ', χ'') were fitted simultaneously. If it was noticed that β was close to 1, then the fitting was repeated with β fixed to 1 (one Debye process). We found that for zero DC bias field all curves could be relatively well fitted with one Debye process. At 1000 Oe the situation is different. In this case all curves could be well fitted with two Debye processes. All fitting details are collected in Table S5 and S6 in the Supporting Information. In Figure 12

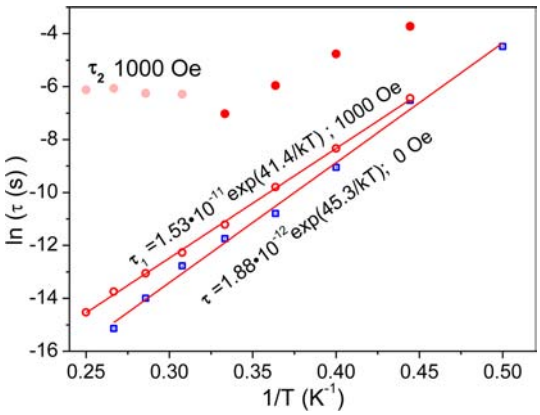

Figure 12. Reciprocal temperature dependences of the logarithm of the relaxation time in two DC fields for **3** (see text). τ refers to the field of 5 Oe. The two relaxation times, discernible in 1000 Oe, are labeled as τ_1 and τ_2. The pale points of τ_2 left of the minimum are not reliable because the contribution of the corresponding process above 3 K is very small. Solid lines are linear fits.

dx.doi.org/10.1021/ic4012235 | Inorg. Chem. 2013, 52, 12947−12957

the reciprocal temperature dependences of the logarithm of relaxation time are shown. It is seen that relaxation times, τ in 5 Oe and τ_1 in 1000 Oe, obey the Arrhenius equation

$$\tau = \tau_0 e^{\Delta_\tau / kT} \quad (8)$$

The second relaxation time τ_2, discernible at 1000 Oe, has a peculiar temperature dependence with a minimum at 3.0 K. However, the points to the left of the minimum (red pale points) are not reliable because the contribution of this relaxation process is very small above 3 K, $\beta \approx 0.98$ (see Supporting Information, Table S6). The relaxation process in a field of 5 Oe (τ) does not much differ from that in 1000 Oe (τ_1). The corresponding two lines in Figure 12 are nearly parallel and close to each other. This proves that the relaxation process in 1000 Oe is the same as that in 5 Oe. For this process the energy barrier Δ_τ for the magnetization reversal is ~45 K, and the pre-exponential factor τ_0 equals 1.9×10^{-12} s (in 5 Oe). The parameter α changes with temperature obtaining the quite large value of ~0.4 for 5 Oe and 0.3 for 1000 Oe at the lowest temperatures (see Tables S5 and S6 in the Supporting Information).

Relevant parameters of **3** are collected in Table 1. The Mydosh-parameter φ, defined as the temperature shift of the χ''

Table 1. Magnetic Parameters of $[Co(NCS)_2(4\text{-ethylpyridine})_2]_n$

	$[Co(NCS)_2(4\text{-ethylpyridine})_2]_n$
T_N (K)[a]	3.4
H_c (Oe) at 2 K	175
J_{intra} (K) (S = 1/2)	25.2
zJ' (K)	−0.28
φ	0.14
α in 5 Oe[b]	0.1−0.4
τ_0 (s) in 5 Oe	1.9×10^{-12}
Δ_τ (K) in 5 Oe	45.3

[a] T_N is the Neel point. [b] α is temperature dependent.

peak on the decade of frequency $(\Delta T_p/T_p)/\Delta(\log 2\pi f)$, equals to 0.14, thus is in the range typical for SCM and superparamagnets.[16]

Phase Diagram. A series of field and temperature dependent measurements was performed to construct the phase diagram. To this end we used the AC susceptibility method, similarly as done by van Duyneveldt et al. for single crystal samples.[17] Some data were taken also from DC magnetization measurements. The AC data that we used are shown in Figure 13. They were obtained as a function of external field at various temperatures for the amplitude and frequency of the driving magnetic field of 3 Oe and 10 Hz, respectively.

The data for 2.0, 2.5, and 3.0 K were obtained both with increasing and decreasing magnetic field. As seen, these data show a small irreversibility at the field range of the double maximum, which is clearly seen for T = 3 K. There is, however, no irreversibility at the critical field, which was expected on the basis of DC measurements. The data were differentiated and some representative derivative curves are shown in Figure S19 in the Supporting Information. The characteristic points, that we used, are the maxima at about 200 and 500 Oe and a minimum at about 750 Oe. The phase diagram built on the basis of these points is shown in Figure 14. The bottom horizontal line is the H_C line, the next line above it (blue

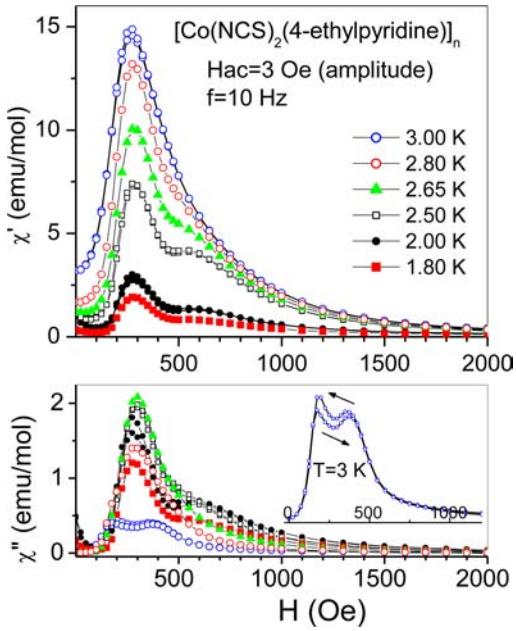

Figure 13. χ' and χ'' AC susceptibility components registered as a function of the external DC field for frequency of 10 Hz at various temperatures. The measurement for T = 2.0, 2.5, and 3.0 K was performed with increasing and decreasing field. The data for χ'' at 3 K are separately shown in another scale.

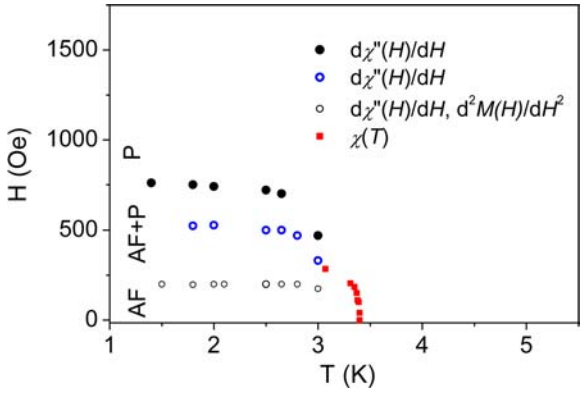

Figure 14. Applied magnetic field vs temperature phase diagram for a powder sample of **3**. AF = antiferromagnetic phase, P is paramagnetic phase, and AF+P represents the mixed phase. Different symbols denote the different origin of data points.

points), corresponding to the second χ' or χ'' maximum, most likely represents the critical field line, related with the presence of a second direction of the easy anisotropy axis (see Figure 4). The upper line represents the boundary between mixed and pure saturated paramagnetic phase; see refs 17a−c. This mixed phase appears because of demagnetizations effects, so that the metamagnetic transition is not sudden and the antiferromagnetic phase gradually transforms with increasing external field to the saturated paramagnetic phase. During this transformation the internal field remains constant.[17a−c] The red points near the Néel temperature on the diagram were obtained from the maximum of the $\chi(T)$ curve, that is, from DC measurements in various field.

It is interesting to compare the data obtained from first field derivative of AC susceptibility with those obtained from the second field derivative of the magnetization shown in Figures S19 and S20 in the Supporting Information, respectively. They

dx.doi.org/10.1021/ic4012235 | Inorg. Chem. 2013, 52, 12947−12957

are similar—some points on the H_C line in the diagram taken from the AC method are the same as ones taken from the $\partial^2 M/\partial H^2$ curve. However, there is some difference for the lowest fields below ~150 Oe and for temperatures below 2.5 K. As mentioned before, the hysteresis loop remains open by decreasing field down to 0 Oe. This is reflected on the $\partial^2 M/\partial H^2$ curve and even better on the $\partial M/\partial H$ curves (see Figure S15 in the Supporting Information for T = 2 and 2.3 K) but no sign of this effect is seen on the $\partial\chi'/\partial H$ or $\partial\chi''/\partial H$. As mentioned above, the AC data are reversible at the critical field, which means that a slow relaxation process exists, which is not detectable in the frequency window of the AC method.

DISCUSSION

The magnetic investigations presented above clearly show that the ground state of **3** is antiferromagnetic with a Néel temperature T_N of 3.4 K. The magnetic structure of **3** consists of ferromagnetic chains, which are weakly antiferromagnetically coupled. Thus, **3** is a quasi 1D magnet with a $|J_{inter}/J_{intra}|$ ratio of about 1×10^{-2}. It is noted that for a comparable ratio a single mode of relaxations was reported[10] but according to Cangussu et al., a small $|J_{inter}/J_{intra}|$ ratio and high easy axis anisotropy may be not sufficient for obtaining SCM properties.[18]

The relaxation properties of **3** are complex. In a zero or small bias DC field the relaxation of magnetization coexists with antiferromagnetic ordering, and this can be traced back to the relaxation of single chains. With increasing field a metamagnetic transition starts at a critical field H_C ~175 Oe. However, this relaxation is observed also above H_C at temperatures near 2.5–3 K (Figure 10). Based on the results shown in Figure 12 it can be concluded that the relaxations observed in the antiferromagnetic state survive above the critical field and are still present even in the saturated paramagnetic phase (in field of 1000 Oe).

The relaxation behavior of **3** differs from that known for typical SCMs because of the broad relaxation time distribution (large α) and its dependence on temperature. Two examples from the literature are worth invoking. A paper of Zhang et al. has recently appeared in which a new SCM material was described that is built of ferromagnetic chains of Co(II) ions linked by mixed azide-carboxylate bridges.[19] This compound exhibits antiferromagnetism at T_N = 6.5 K, a metamagnetic transition at ~100 Oe, and also shows the slow dynamics of single chains, which is present in the antiferromagnetic as well as in the field induced state. From a fit to the generalized Debye model a value of α equal to 0.47 in zero field was obtained, which is comparable to our value and which suggests a large distribution of the relaxation times. A bifurcation FC vs ZFC was also observed in the antiferromagnetic state at a small field of 20 Oe, and the $M(H)$ curve showed a hysteresis loop between 0.5 and 15 kOe. Thus, this overall behavior is similar to the behavior of **3**, the essential difference is that in **3** the hysteresis loops remains open down to 0 Oe.

Another example is $Co(Cl)_2(pyridine)_2$, which has a structure similar to that of **3**. It is composed of ferromagnetic chains in which the Co(II) cations are octahedrally coordinated by four chlorine atoms and two pyridine ligands and are connected via common edges of chlorine atoms. This compound is an antiferromagnet with $T_N \approx 3.0$ K, that shows a two-step metamagnetic transition at 0.8 and 1.6 kOe.[12] It is expected that the relaxation behavior of $Co(Cl)_2(pyridine)_2$ may be similar to that of **3**. This behavior was studied in zero DC field by Elmassalami and de Jongh and was explained by the presence of single π kinks and kink-pairs propagating in chains or in other words, single and paired Bloch walls.[20] We suggest that in our case an interaction of kinks between neighboring chains could lead to the broad distribution of the relaxation times.

Assuming that the mean relaxation time τ determined for 5 Oe corresponds to the relaxations of single chains, the contribution of the anisotropy can be estimated applying the equation[1d]

$$\Delta_\tau = n\Delta_\xi + \Delta_A \quad (9)$$

where Δ_τ is the activation energy of the relaxation time, Δ_ξ is the creation energy of the domain wall given by the relation $\chi T \propto \exp(\Delta_\xi/kT)$, and Δ_A is the activation energy of a single anisotropic spin inside a narrow domain wall (where it sees no local field). n is a factor equal to 1 or 2 depending on whether chains are finite or infinite, respectively. By eq 2, $\Delta_\xi = J/2$. Substituting Δ_τ = 45.3 K and Δ_ξ = 12.6 K to eq 9 and assuming infinite chains (n = 2, AC regime) a value for Δ_A of 20.1 K is obtained. Unfortunately, we have no independent estimation of this anisotropy parameter, but this value is in rough agreement with that reported by Zhang et al. of Δ_A = 10 K for the Co(II) chain compound mentioned above. Moreover, Zhang et al. found a similar value for the activation energy (Δ_τ = 49 K) but a different value for Δ_ξ of 39 K.[19]

AC measurements have shown that the relaxation processes in **3** (τ and τ_1 in Figure 13) observed by this method are relatively fast and cannot contribute to the observed bifurcations and hysteresis loop. The relaxation times derived from the AC method are much lower than 1 s at 2 K. In contrast, the relaxation rates measured by the DC method are much slower (~12 min) and seem to be related with an additional relaxation process of larger objects, such as ferromagnetically aligned 3D domains. Such domains are expected in the mixed AF+P phase, which appears above H_C. However, in **3** they appear in the metamagnetic transition above H_C and decay with decreasing field but persist down to 0 Oe. The reason why domains do not disappear completely at H_C with decreasing field is not clear and needs further investigation.

As mentioned in the introduction these investigations were performed as a part of a larger project on the magnetic properties of Co(II) thio- and selenocyanato coordination polymers. In the present study we investigated for the first time the influence of the coligand and therefore, pyridine was exchanged by 4-ethylpyridine. In this case remarkable differences are found because in contrast to the pyridine compound a metamagnetic transition occurs.[7] Moreover, whereas the magnetic ground state in **3** is antiferromagnetic our previous investigations indicate that it is ferromagnetic in the pyridine compound. This might be traced back to the different packing of the individual chains which is different in both compounds. In this context it is noted that according to Elmassalami and de Jongh the anisotropy axis in $Co(Cl)_2(pyridine)_2$ is directed along the N–Co–N direction;[20a] thus, the same is expected in the thiocyanato compounds **3** and $[Co(NCS)_2(pyridine)_2]_n$. In contrast to the latter compound particular chains have differently oriented organic ligands (see Figure 4) and therefore, the magnetic structure of **3** may be noncollinear, which is not the case for the pyridine compound.

Fortunately, the slow relaxations still remain after ligand exchange, which strongly indicates that these compounds are part of a very stable system, in which the components can be

dx.doi.org/10.1021/ic4012235 | Inorg. Chem. 2013, 52, 12947–12957

exchanged to some extent without losing this interesting behavior. Consequently, a versatile model system was found in which the influence of a chemical modification on the magnetic properties of this class of compounds can be investigated in more detail. However, as mentioned above, the present findings clearly show that the relaxation behavior is not pure SCM behavior, which is especially indicated by the large and temperature dependent α values. In contrast, the relaxations in the pyridine compound were interpreted only as SCM relaxations as indicated by the low α value determined at only one field and only one temperature and similar observations were made for related compounds reported recently. However, our new findings suggest that even for the pyridine compound interchain interactions cannot be neglected and therefore, a more detailed study on the magnetic properties of this compound is really needed. More generally, it is also highly likely that all members of this class of compounds show a similar behavior. At higher temperatures they might show the magnetic behavior of individual chains, but especially at low temperatures interchain interactions cannot be neglected which would lead to a more complex magnetic behavior as it is observed in the present study. If this is really the case will be the subject of further investigations.

EXPERIMENTAL SECTION

Materials. $Co(NCS)_2$ and 4-ethylpyridine were obtained from Alfa Aesar and were used without further purification. All crystalline powders were prepared by stirring the reactants for 3 days at room-temperature. The obtained residues were filtered off and washed with water and diethyl ether and dried in vacuum. The purity was checked by XRPD and elemental analysis.

Table 2. Selected Crystal Data and Details on the Structure Determination from Single Crystal Data for All Compounds

	1	2	3
formula	$C_{30}H_{36}CoN_6S_2$	$C_{46}H_{54}Co_2N_{10}S_4$	$C_{16}H_{18}CoN_4S_2$
MW/g·mol^{-1}	603.70	993.09	389.39
crystal system	triclinic	orthorhombic	monoclinic
space group	$P\bar{1}$	*Pbca*	*Cc*
a /Å	10.3959(4)	15.5182(9)	11.2697(6)
b/Å	16.2297(5)	11.4066(4)	39.566(3)
c/Å	20.0857(6)	27.9992(10)	9.1863(5)
α/deg	91.529(3)	90	90
β/deg	90.820(3)	90	115.230(6)
γ/deg	103.129(3)	90	90
V/Å^3	3298.43(19)	4956.1(4)	3705.4(4)
T/K	293	200	200
Z	4	4	8
D_{calc}/mg·m^3	1.216	1.331	1.396
μ/mm^{-1}	0.674	0.880	1.155
θ_{max}/deg	25.01	25.00	27.50
refl. collected	38963	17474	16964
unique reflections	11555	4366	8023
R_{int}	0.0273	0.0767	0.0542
refl. [$F_o > 4\sigma(F_o)$]	8559	2685	6446
parameters	700	283	425
R_1 [$F_o > 4\sigma(F_o)$]	0.0617	0.0404	0.0410
wR_2	0.1746	0.0914	0.1027
GOF	1.049	0.954	0.960
$\Delta\rho_{max/min}$/e·Å^{-3}	0.515/−0.333	0.383/−0.287	0.416/−0.468

Synthesis of $[Co(NCS)_2(4\text{-ethylpyridine})_4]$ (1). A red crystalline powder was prepared by the reaction of $Co(NCS)_2$ (1.50 mmol, 261 mg) and 4-ethylpyridine (6.00 mmol, 682 μL) in 10 mL of water in a snap cap vial. Yield based on $Co(NCS)_2$: 883 mg (97.6%). Elemental analysis for $C_{30}H_{36}CoN_6S_2$ (603.72) calcd.: C 59.68, H 6.01, N 13.92, S 10.62 ; found: C 59.70, H 6.03, N 13.91, S 10.64. IR: ν_{max} = 2970 (w), 2057 (s), 1612 (s), 1557 (w), 1500 (w), 1424 (m), 1221 (m), 1069 (w), 1016 (m), 829 (s), 787 (m), 573 (m), 502 (m) cm^{-1} (Figure S1 in the Supporting Information). Single-crystals suitable for X-ray structure determination were obtained by a reaction of $Co(NCS)_2$ (0.15 mmol, 26.1 mg) and 4-ethylpyridine (0.6 mmol, 68.2 μL) in 1 mL of acteonitrile in a closed snap cap vial. Red block-shaped single-crystals were obtained after 3 days.

Synthesis of $[(Co(NCS)_2]_2(4\text{-ethylpyridine})_6$ (2). A light-red crystalline powder was prepared by the reaction of $Co(NCS)_2$ (1.50 mmol, 261 mg) and 4-ethylpyridine (1.50 mmol, 171 μL) in 10 mL of water in a snap cap vial. Yield based on $Co(NCS)_2$: 709 mg (95.3%). Elemental analysis for $C_{23}H_{27}CoN_5S_2$ (496.56) calcd.: C 55.63, H 5.48, N 14.10, S 12.92; found: C 55.61, H 5.45, N 14.11, S 12.91. IR: ν_{max} = 2969 (w), 2111 (s), 2066 (s), 1615 (s), 1555 (w), 1501 (w), 1423 (m), 1225 (m), 1066 (w), 1018 (m), 827 (s), 785 (m), 577 (m), 498 (m) cm^{-1} (Figure S2 in the Supporting Information). Single-crystals suitable for X-ray structure determination were obtained by a reaction of $Co(NCS)_2$ (0.15 mmol, 26.1 mg) and 4-ethylpyridine (0.15 mmol, 17.1 μL) in 1 mL of water in a closed snap cap vial. Light-red block-shaped single-crystals were obtained after 1 day.

Synthesis of $[Co(NCS)_2(4\text{-ethylpyridine})_2]_n$ (3). A pink crystalline powder was prepared by the reaction of $Co(NCS)_2$ (6.00 mmol, 1050 mg) and 4-ethylpyridine (1.5 mmol, 171 μL) in 10 mL of water in a snap cap vial. Yield based on $Co(NCS)_2$: 571 mg (97.8%). Elemental analysis for $C_{16}H_{18}N_4CoS_2$ (389.41) calcd.: C 49.35, H 4.66, N 15.13, S 16.47; found: C 49.32, H 4.64, N 15.10, S 16.45. IR: ν_{max} = 2969 (w), 2100 (s), 1614 (s), 1422 (m), 1225 (m), 1019 (m), 825 (s), 787 (m), 571 (s), 510 (s), 468 (s) cm^{-1} (Figure S3 in the Supporting Information). Single-crystals suitable for X-ray structure determination were obtained by a reaction of $Co(NCS)_2$ (0.90 mmol, 158 mg) and 4-ethylpyridine (0.15 mmol, 17.1 μL) in 1 mL of water under hydrothermal condition at 120 °C. Pink block-shaped single-crystals were obtained after 1 day on cooling.

C, H, N, S Analysis. CHNS analysis was performed using an EURO EA elemental analyzer, fabricated by EURO VECTOR Instruments and Software.

Spectroscopy. All IR data were obtained using an ATI Mattson Genesis Series FTIR Spectrometer, control software: WINFIRST, from ATI Mattson.

X-ray Powder Diffraction (XRPD). The measurements were performed using (1) a PANalytical X'Pert Pro MPD Reflection Powder Diffraction System with CuKα1 radiation (λ = 154.0598 pm) equipped with a PIXcel semiconductor detector from PANanlytical and (2) a Stoe Transmission Powder Diffraction System (STADI-P) with CuKα1 radiation (λ = 154.0598 pm) that was equipped with a linear position-sensitive detector from STOE & CIE.

Magnetic Measurements. The magnetic measurements were performed on polycrystalline samples using a PPMS (Physical Property Measurement System) from Quantum Design, equipped with a 9 Tesla magnet. Some measurements were also performed with a LakeShore AC-susceptometer/DC-magnetometer, model 7225 and with a Quantum Design Squid magnetometer, model XPMS-XL5. The samples were strongly hand pressed and for some measurements the samples were frozen in Nujol. Diamagnetic corrections were applied with the use of the tabulated Pascal's constants.

Single-Crystal Structure Analysis. Single-crystal data collections were carried out on an imaging plate diffraction system: Stoe IPDS-1 for **2** and **3** as well as Stoe IPDS-2 for **1** with MoKα radiation. The structures were solved with direct methods using SHELXS-97 and structure refinements were performed against F^2 using SHELXL-97.[21] Numerical absorption correction was applied using programs X-RED and X-SHAPE of the program package X-Area.[22] All non hydrogen atoms were refined with anisotropic displacement parameters. All hydrogen atoms were positioned with idealized geometry and were refined isotropic with $U_{iso}(H) = 1.2U_{eq}(C)$ (1.5 for methyl H atoms) using a riding model. The crystal of compound **3** was racemically

dx.doi.org/10.1021/ic4012235 | *Inorg. Chem.* 2013, 52, 12947−12957

twinned, and therefore a twin refinement was performed (BASF parameter: 0.71 (2). In this compound one ethyl group is disordered and was refined using a split model. Details of the structure determination are given in Table 2.

CCDC 967788 (**1**), CCDC 967789 (**2**), and CCDC 967790 (**3**) contain the supplementary crystallographic data for this paper. These data can be obtained free charge from the Cambridge Crystallographic Data Centre via http://www.ccdc.cam.ac.uk/data_request/cif.

Differential Thermal Analysis and Thermogravimetry (DTA-TG). The DTA-TG measurements were performed in a nitrogen atmosphere (purity: 5.0) in Al_2O_3 crucibles using a STA-409CD instrument from Netzsch. All measurements were performed with a flow rate of 75 mL·min^{-1} and were corrected for buoyancy and current effects. The instrument was calibrated using standard reference materials.

■ ASSOCIATED CONTENT

Ⓢ Supporting Information

IR spectra of compound **1**, **2**, and **3**, DTA/TG/DTG measurements of compound **1**, experimental XRPD measurements of compound **1**, **2**, and **3**, ORTEP plots of compound **1**, **2**, and **3**, magnetic measurements of compound **1**, **2**, and **3**, as well as selected bond lengths and angles of compound **1**, **2**, and **3**. This material is available free of charge via the Internet at http://pubs.acs.org.

■ AUTHOR INFORMATION

Corresponding Author

*E-mail: cnaether@ac.uni-kiel.de. Fax: +49-431-8801520.

Notes

The authors declare no competing financial interest.

■ ACKNOWLEDGMENTS

This project was supported by the *Deutsche Forschungsgemeinschaft* (Project No. NA 720/5-1) and the State of Schleswig-Holstein. We thank Prof. Dr. Wolfgang Bensch from the University of Kiel for access to his experimental facilities. Special thanks go to Inke Jess, Henning Lühmann, and Maren Rasmussen. Z.T. acknowledges the Grant of NCN Poland N N202103328.

■ REFERENCES

(1) (a) Sun, H.-L.; Wang, Z.-M.; Gao, S. *Coord. Chem. Rev.* **2010**, *254* (9−10), 1081−1100. (b) Miyasaka, H.; Clérac, R. *Bull. Chem. Soc. Jpn.* **2005**, *78* (10), 1725−1748. (c) Bogani, L.; Vindigni, A.; Sessoli, R.; Gatteschi, D. *J. Mater. Chem* **2008**, *18* (40), 4733−4880. (d) Coulon, C.; Miyasaka, H.; Clérac, R. *Struct. Bonding (Berlin)* **2006**, *122*, 163−206. (e) Leuenberger, M. N.; Loss, D. *Nature* **2001**, *410* (6830), 789−793. (f) Sessoli, R. *Angew. Chem.* **2012**, *124* (1), 43−45. (g) Miller, J. S.; Epstein, A. J. *Angew. Chem., Int. Ed. Engl.* **1994**, *33* (4), 385−415. (h) Aromi, G.; Aguila, D.; Gamez, P.; Luis, F.; Roubeau, O. *Chem. Soc. Rev.* **2012**, *41* (2), 537−546. (i) Mas-Ballesté, R.; Gómez-Herrero, J.; Zamora, F. *Chem. Soc. Rev.* **2010**, *39* (11), 4220−4233. (j) Kiebach, R.; Näther, C.; Kögerler, P.; Bensch, W. *Dalton Trans.* **2007**, No. 30, 3221−3223. (k) Zheng, Y.-Z.; Speldrich, M.; Schilder, H.; Chen, X.-M.; Kögerler, P. *Dalton Trans.* **2010**, *39* (45), 10827−10829. (l) Ferrando-Soria, J.; Cangussu, D.; Eslava, M.; Journaux, Y.; Lescouëzec, R.; Julve, M.; Lloret, F.; Pasán, J.; Ruiz-Pérez, C.; Lhotel, E.; Paulsen, C.; Pardo, E. *Chem.—Eur. J.* **2011**, *17* (44), 12482−12494. (m) Lescouëzec, R.; Toma, L. M.; Vaissermann, J.; Verdaguer, M.; Delgado, F. S.; Ruiz-Pérez, C.; Lloret, F.; Julve, M. *Coord. Chem. Rev.* **2005**, *249* (23), 2691−2729.

(2) Caneschi, A.; Gatteschi, D.; Lalioti, N.; Sangregorio, C.; Sessoli, R.; Venturi, G.; Vindigni, A.; Rettori, A.; Pini, M. G.; Novak, M. A. *Angew. Chem., Int. Ed.* **2001**, *40* (9), 1760−1763.

(3) (a) Zhao, J.-P.; Yang, Q.; Liu, Z.-Y.; Zhao, R.; Hu, B.-W.; Du, M.; Chang, Z.; Bu, X.-H. *Chem. Commun.* **2012**, *48* (52), 6568−6570. (b) Yang, C.-I.; Chuang, P.-H.; Lu, K.-L. *Chem. Commun.* **2011**, *47* (15), 4445−4447. (c) Luo, F.; Liao, Z.-w.; Song, Y.-m.; Huang, H.-x.; Tian, X.-z.; Sun, G.-m.; Zhu, Y.; Yuan, Z.-Z.; Luo, M.-b.; Liu, S.-j.; Xu, W.-y.; Feng, X.-F. *Dalton Trans.* **2011**, *40* (47), 12651−12655. (d) Kar, P.; Biswas, R.; Drew, M. G. B.; Ida, Y.; Ishida, T.; Ghosh, A. *Dalton Trans.* **2011**, *40* (13), 3295−3304. (e) Ferrando-Soria, J.; Pardo, E.; Ruiz-García, R.; Cano, J.; Lloret, F.; Julve, M.; Journaux, Y.; Pasán, J.; Ruiz-Pérez, C. *Chem.—Eur. J.* **2011**, *17* (7), 2176−2188. (f) Tomkowicz, Z.; Rams, M.; Bałanda, M.; Foro, S.; Nojiri, H.; Krupskaya, Y.; Kataev, V.; Büchner, B.; Nayak, S. K.; Yakhmi, J. V.; Haase, W. *Inorg. Chem.* **2012**, *51* (18), 9983−9994. (g) Bałanda, M.; Tomkowicz, Z.; Haase, W.; Rams, M. *J. Phys.: Conf. Ser.* **2011**, *303*, 012036. (h) Bałanda, M.; Rams, M.; Nayak, S. K.; Tomkowicz, Z.; Haase, W.; Tomala, K.; Yakhmi, J. V. *Phys. Rev. B* **2006**, *74* (22), 224421. (i) Palii, A. V.; Reu, O. S.; Ostrovsky, S. M.; Klokishner, S. I.; Tsukerblat, B. S.; Sun, Z.-M.; Mao, J.-G.; Prosvirin, A. V.; Zhao, H.-H.; Dunbar, K. R. *J. Am. Chem. Soc.* **2008**, *130* (44), 14729−14738. (j) Shatruk, M.; Avendano, C.; Dunbar, K. R. Cyanide-Bridged Complexes of Transition Metals: A Molecular Magnetism Perspective. In *Progress in Inorganic Chemistry*; John Wiley & Sons, Inc.: New York, 2009; pp 155−334; (k) Feng, X.; David Harris, T.; Long, J. R. *Chem. Sci.* **2011**, *2* (9), 1688−1694. (l) Feng, X.; Liu, J.; Harris, T. D.; Hill, S.; Long, J. R. *J. Am. Chem. Soc.* **2012**, *134* (17), 7521−7529. (m) Zhang, S.-Y.; Shi, W.; Lan, Y.; Xu, N.; Zhao, X.-Q.; Powell, A. K.; Zhao, B.; Cheng, P.; Liao, D.-Z.; Yan, S.-P. *Chem. Commun.* **2011**, *47* (10), 2859−2861. (n) Hu, S.; Liu, J.-L.; Meng, Z.-S.; Zheng, Y.-Z.; Lan, Y.; Powell, A. K.; Tong, M.-L. *Dalton Trans.* **2011**, *40* (1), 27−30. (o) Zhang, W.-X.; Ishikawa, R.; Breedlovea, B.; Yamashita, M. *RSC Adv.* **2013**, *3*, 3772−3798.

(4) (a) Wöhlert, S.; Wriedt, M.; Fic, T.; Tomkowicz, Z.; Haase, W.; Näther, C. *Inorg. Chem.* **2013**, *52* (2), 1061−1068. (b) Wöhlert, S.; Fink, L.; Schmidt, M.; Näther, C. *CrystEngComm* **2013**, *15*, 945−957. (c) Näther, C.; Greve, J. *J. Solid State Chem.* **2003**, *176* (1), 259−265. (d) Wriedt, M.; Sellmer, S.; Näther, C. *Dalton Trans.* **2009**, No. 38, 7975−7984. (e) Wriedt, M.; Sellmer, S.; Näther, C. *Inorg. Chem.* **2009**, *48* (14), 6896−6903. (f) Wriedt, M.; Jeß, I.; Näther, C. *Eur. J. Inorg. Chem.* **2009**, No. 10, 1406−1413.

(5) (a) Vujovic, D.; Raubenheimer, H. G.; Nassimbeni, L. R. *Dalton Trans.* **2003**, No. 4, 631−637. (b) Sekiya, R.; Nishikiori, S.-i. *CrystEngComm* **2011**, *13* (21), 6405−6414. (c) Shi, J. M.; Chen, J. N.; Wu, C. J.; Ma, J. P. *J. Coord. Chem.* **2007**, *60* (18), 2009−2013. (d) Jin, Y.; Che, Y.-x.; Zheng, J.-m. *J. Coord. Chem.* **2007**, *60* (19), 2067−2074.

(6) (a) Boeckmann, J.; Näther, C. *Chem. Commun.* **2011**, *47* (25), 7104−7106. (b) Wöhlert, S.; Boeckmann, J.; Jess, I.; Näther, C. *CrystEngComm* **2012**, *14*, 5412−5420. (c) Boeckmann, J.; Näther, C. *Polyhedron* **2012**, *31*, 587−595. (d) Grossmann, H.; Hünseler, F. *Z. Anorg. Chem.* **1905**, *46* (1), 361−405. (e) Huang, W.; Ogawa, T. *J. Mol. Struct.* **2006**, *785* (1−3), 21−26. (f) Valach, F.; Sivy, P.; Koren, B. *Acta Crystallogr.* **1984**, *C40* (6), 957−959. (g) Yang, H.; Chen, Y.; Li, D.; Wang, D. *Acta Crystallogr.* **2007**, *E63* (12), m3186. (h) Reller, A.; Oswald, H.-R. *J. Solid State Chem.* **1986**, *62* (3), 306−316.

(7) Boeckmann, J.; Näther, C. *Dalton Trans.* **2010**, *39* (45), 11019.

(8) (a) Wöhlert, S.; Boeckmann, J.; Wriedt, M.; Näther, C. *Angew. Chem., Int. Ed.* **2011**, *50* (30), 6920−6923. (b) Wöhlert, S.; Ruschewitz, U.; Näther, C. *Cryst. Growth Des.* **2012**, *12* (6), 2715−2718.

(9) Miyasaka, H.; Takayama, K.; Saitoh, A.; Furukawa, S.; Yamashita, M.; Clérac, R. *Chem.—Eur. J.* **2010**, *16* (12), 3656−3662.

(10) Coulon, C.; Clérac, R.; Wernsdorfer, W.; Colin, T.; Miyasaka, H. *Phys. Rev. Lett.* **2009**, *102* (16), 164204−164207.

(11) (a) Keene, T. D.; Zimmermann, I.; Neels, A.; Sereda, O.; Hauser, J.; Bonin, M.; Hursthouse, M. B.; Price, D. J.; Decurtins, S. *Dalton Trans.* **2010**, *39* (20), 4937−4950. (b) Przybylak, S. W.; Tuna, F.; Teat, S. J.; Winpenny, R. E. P. *Chem. Commun.* **2008**, No. 17, 1983−1985. (c) Boeckmann, J.; Wriedt, M.; Näther, C. *Chem.—Eur. J.* **2012**, *18* (17), 5284−5289.

(12) (a) Foner, S.; Frankel, R. B.; McNiff, J. E. J.; Reiff, W. M.; Little, B. F.; Long, G. J. *AIP Conf. Proc.* **1975**, *24* (1), 363−364. (b) Foner, S.; Frankel, R. B.; Reiff, W. M.; Little, B. F.; Long, G. J. *Solid State Commun.* **1975**, *16*, 159−161. (c) Foner, S.; Frankel, R. B.; Reiff, W. M.; Wong, H.; Long, G. J. *J. Chem. Phys.* **1978**, *68*, 4781−4783.
(13) (a) Mukherjee, A. K.; Nayak, N. P.; Mondal, A.; Chaudhuri, N. R. *Acta Crystallogr.* **1999**, *55* (3), 365−368. (b) Boeckmann, J.; Evers, N.; Nather, C. *CrystEngComm* **2012**, *14* (3), 1094−1104. (c) Lipkowski, J.; Andreetti, G. *Transition Met. Chem.* **1978**, *3* (1), 117−121. (d) Małecki, J. G.; Świtlicka, A.; Groń, T.; Bałanda, M. *Polyhedron* **2010**, *29* (17), 3198−3206. (e) Bhowmik, P.; Chattopadhyay, S.; Drew, M. G. B.; Diaz, C.; Ghosh, A. *Polyhedron* **2010**, *29* (13), 2637−2642. (f) Hermann, G.; Fritz, H. Über die Verbindungen der Metallrhodanide mit organischen Basen *Z. Anorg. Allg. Chem.* [Online], **1905**, pp 361−405; http://dx.doi.org/10.1002/zaac.19050460122.
(14) Fisher, M. E. *J. Math. Phys.* **1963**, *4*, 124−135.
(15) (a) Carlin, R. L.; van Duyneveldt, A. J., *Magnetic properties of transition metal compounds*; Springer Verlag: Berlin, Germany, 1977; Vol. 2; (b) Scalapino, D. J.; Imry, Y.; Pincus, P. *Phys. Rev. B* **1975**, *11* (5), 2042−2048.
(16) (a) Ishii, N.; Okamura, Y.; Chiba, S.; Nogami, T.; Ishida, T. *J. Am. Chem. Soc.* **2008**, *130* (1), 24−25. (b) Sun, H.-L.; Wang, Z.-M.; Gao, S. *Chem.—Eur. J.* **2009**, *15* (7), 1757−1764. (c) Liu, T.-F.; Fu, D.; Gao, S.; Zhang, Y.-Z.; Sun, H.-L.; Su, G.; Liu, Y.-J. *J. Am. Chem. Soc.* **2003**, *125* (46), 13976−13977.
(17) (a) Carlin, R. L.; van Duyneveldt, A. J. *Acc. Chem. Res.* **1980**, *13* (7), 231−236. (b) Hoogerbeets, R.; Wiegers, S. A. J.; van Duyneveldt, A. J.; Willett, R. D.; Geiser, U. *Phys. B* **1984**, *125* (2), 135−149. (c) Groenendijk, H. A.; Blöte, H. W. J.; van Duyneveldt, A. J.; Gaura, R. M.; Landee, C. P.; Willett, R. D. *Phys. B* **1981**, *106* (1), 47−58. (d) Groenendijk, H. A.; Van Duyneveldt, A. J. *Phys. B* **1982**, *115* (1), 41−62.
(18) Cangussu, D.; Nunes, W. C.; Pereira, C. L. M.; Pedroso, E. F.; Mazali, I. O.; Knobel, M.; Alves, O. L.; Stumpf, H. O. *Eur. J. Inorg. Chem.* **2008**, *2008* (24), 3802−3808.
(19) Zhang, X.-M.; Wang, Y.-Q.; Wang, K.; Gao, E.-Q.; Liu, C.-M. *Chem. Commun.* **2011**, *47* (6), 1815−1817.
(20) (a) ElMassalami, M.; de Jongh, L. J. *Phys. B* **1989**, *154* (2), 254−266. (b) de Jongh, L. J. *J. Appl. Phys.* **1982**, *53*, 8018−8023. (c) de Jongh, L. J.; Mulder, C. A. M.; Cornelisse, R. M.; van Duyneveldt, A. J.; Renard, J. P. *Phys. Rev. Lett.* **1981**, *47* (23), 1672−1675.
(21) Sheldrick, G. M. *Acta Crystallogr.* **2008**, *A64*, 112−122.
(22) (a) *X-Red, Program for Data Reduction and Absorption Correction*, Version 1.11; STOE & CIE GmbH: Darmstadt, Germany, 1998; (b) *X-Shape, Program for the Crystal Optimization for Numerical Absorption Correction*, Version 1.03; STOE & CIE GmbH: Darmstadt, Germany, 1998; (c) *X-Area, Program Package for Single Crystal Measurements*, Version 1.44; STOE & CIE GmbH: Darmstadt, Germany, 2008.